



# Fabrication of $\text{WO}_3 \cdot 2\text{H}_2\text{O}/\text{BC}$ Hybrids by the Radiation Method for Enhanced Performance Supercapacitors

Fan Yang<sup>1†</sup>, Jinzhi Jia<sup>1,2†</sup>, Rui Mi<sup>1</sup>, Xichuan Liu<sup>1</sup>, Zhibing Fu<sup>1</sup>, Chaoyang Wang<sup>1</sup>, Xudong Liu<sup>1,3\*</sup> and Yongjian Tang<sup>1\*</sup>

<sup>1</sup> Science and Technology on Plasma Physics Laboratory, Research Centre of Laser Fusion, China Academy of Engineering Physics, Mianyang, China, <sup>2</sup> School of Materials Science and Engineering, Southwest University of Science and Technology, Mianyang, China, <sup>3</sup> College of Materials Science and Engineering, Chongqing University, Chongqing, China

## OPEN ACCESS

### Edited by:

Qiaobao Zhang,  
Xiamen University, China

### Reviewed by:

Shuge Dai,  
Zhengzhou University, China  
Zhao Yan,  
Jiangsu University, China

### \*Correspondence:

Xudong Liu  
8sliuxudong@caep.cn  
Yongjian Tang  
tangyongjian2000@sina.com

<sup>†</sup>These authors have contributed  
equally to this work

### Specialty section:

This article was submitted to  
Nanoscience,  
a section of the journal  
Frontiers in Chemistry

Received: 06 May 2018

Accepted: 25 June 2018

Published: 13 August 2018

### Citation:

Yang F, Jia J, Mi R, Liu X, Fu Z,  
Wang C, Liu X and Tang Y (2018)  
Fabrication of  $\text{WO}_3 \cdot 2\text{H}_2\text{O}/\text{BC}$  Hybrids  
by the Radiation Method for Enhanced  
Performance Supercapacitors.  
Front. Chem. 6:290.  
doi: 10.3389/fchem.2018.00290

In this study, we described a facile process for the fabrication of tungsten oxide dihydrate/bamboo charcoal hybrids ( $\text{WO}_3 \cdot 2\text{H}_2\text{O}/\text{BC}$ ) by the  $\gamma$ -irradiation method. The structural, morphological, and electrochemical properties of  $\text{WO}_3 \cdot 2\text{H}_2\text{O}/\text{BC}$  hybrids were investigated using X-ray diffraction (XRD), field emission scanning electron microscopy (FESEM), transmission electron microscopy (TEM), cyclic voltammetry (CV), galvanostatic charge/discharge (GCD), and electrochemical impedance spectroscopy (EIS) techniques. The combination of BC (electrical double layer charge) and  $\text{WO}_3 \cdot 2\text{H}_2\text{O}$  (pseudocapacitance) created a combined effect, which enhanced the specific capacitance and superior cyclic stability of the  $\text{WO}_3 \cdot 2\text{H}_2\text{O}/\text{BC}$  hybrid electrode. The  $\text{WO}_3 \cdot 2\text{H}_2\text{O}/\text{BC}$  hybrids showed the higher specific capacitance ( $391 \text{ F g}^{-1}$  at  $0.5 \text{ A g}^{-1}$  over the voltage range from  $-1$  to  $0 \text{ V}$ ), compared with BC ( $108 \text{ F g}^{-1}$ ) in  $6 \text{ M KOH}$  solution. Furthermore, the hybrid electrode showed superior long-term performance with 82% capacitance retention even after 10,000 cycles. The experimental results demonstrated that the high performance of  $\text{WO}_3 \cdot 2\text{H}_2\text{O}/\text{BC}$  hybrids could be a potential electrode material for supercapacitors.

**Keywords:**  $\gamma$ -irradiation method,  $\text{WO}_3 \cdot 2\text{H}_2\text{O}/\text{BC}$  hybrids, higher specific capacitance, cyclic stability, supercapacitors

## INTRODUCTION

For the rapid increase of global energy demand and the depletion risk of fossil fuels, developing alternative sustainable, affordable, efficient, and clean energy has become very important (Zhao Y. et al., 2016, 2017; Xu et al., 2017; Yi et al., 2017; Zhao B. et al., 2017). Among energy storage devices, supercapacitors (or ultracapacitors) are promising, owing to their safe operation, super-high service life, and great power density (Wang K. et al., 2014; Dai et al., 2017; Zhao B. et al., 2017; Zhao et al., 2018). They have wide application areas such as electric vehicles, pulse power systems and portable devices (Wang et al., 2018). Depending on the charge storage mechanism, supercapacitors are generally classified into electrical double layer charge (EDLC) and pseudocapacitance charge storage. The former stores charges electrostatically in double layers, whereas the latter stores charges on the surface of the electrode active materials as faradaic redox reactions (Zhang and Park, 2017). In general, carbon-based materials are EDLC type (Pang et al., 2016), whereas transition metal oxides and conducting polymers are pseudocapacitor-type materials (Zhang et al., 2012; Yao C. et al., 2017; Yao S. et al., 2017).

The charge storage of pseudocapacitors is much higher compared to those of EDLCs. More recently, transition metal oxides (i.e., RuO<sub>2</sub>, V<sub>2</sub>O<sub>5</sub>, NiO, MnO<sub>2</sub>, SnO<sub>2</sub>, and WO<sub>3</sub>) have been widely investigated in the applications for supercapacitors, and their charge storage originates from fast superficial redox reactions (Zhu and He, 2012; Zhang et al., 2015; Qiu et al., 2016; Zeng et al., 2017; Zhang and Park, 2017; Liu et al., 2018a). Among many of the reported transition metal oxides, RuO<sub>2</sub> has been considered as the proper material with excellent capacitive performance. However, RuO<sub>2</sub> is expensive and rare, constraining the wide practical applications in electrode materials (Cai et al., 2014). WO<sub>3</sub> is a promising electrode material owing to its various morphologies, high theoretical specific capacitance, environmental friendliness, and low cost (Qiu et al., 2016). Nevertheless, its low electrical conductivity (10<sup>-5</sup>–10<sup>-6</sup> S cm<sup>-1</sup>) has limited the wide applications. If we can improve the conductivity of WO<sub>3</sub>, higher specific capacitances could be achieved as expected. Therefore, many researchers have focused on incorporating WO<sub>3</sub> with highly conductive carbon materials to establish a hybrid-type material that combines advantages of each component (Lu et al., 2012; Xiao et al., 2012; Reddy et al., 2015; Sun et al., 2015; Wang et al., 2015; Yuksel et al., 2016). Wang et al. fabricated the WO<sub>3</sub>/carbon aerogel hybrids with outstanding long-term stability, and the specific capacitance was ~700 F g<sup>-1</sup> (at a scan rate of 25 mV s<sup>-1</sup> in 0.5 M H<sub>2</sub>SO<sub>4</sub> over a voltage window of -0.3 to 0.5 V; Wang Y. H. et al., 2014). Huang et al. also designed graphene-WO<sub>3</sub> hybrids with enhanced supercapacitor capacitance (Xing et al., 2016). Wang et al. fabricated the graphene nanosheets-tungsten oxides with high supercapacitor performance (Wang et al., 2015). Ma et al. fabricated a hybrid based on graphene and WO<sub>3</sub> via the hydrothermal method, which possessed high specific capacitance and superior rate capability (Ma et al., 2015).

Among the conductive materials, activated carbon-based materials are the most promising candidates for supercapacitor applications, due to their unique characteristics of large surface areas, and high electrochemical stability and conductivity (Yang et al., 2014; Li and Wu, 2015; Wang et al., 2016; Boyjoo et al., 2017; Dai et al., 2018). In carbon materials, bamboo charcoal draws research attention for its extraordinarily porous microstructure, cost efficiency, and high absorptive capacity (Wang et al., 2012, 2013, 2016; Zhang et al., 2013; Yang et al., 2014; Li and Wu, 2015; Yu et al., 2015). Li et al. studied the water bamboo-derived porous carbon with a maximum specific capacitance of 268 F g<sup>-1</sup> at a current density of 1 A g<sup>-1</sup> in 6 M KOH electrolyte and good capacity retention of 97.28% even over 5,000 cycles at a current density of 10 A g<sup>-1</sup> (Li and Wu, 2015). Yang et al. also synthesized BC by KOH activation, and the specific capacity retention was more than 91% after 3,000 cycles (Yang et al., 2014). Impressively, BC has long-lasting life, whereas WO<sub>3</sub> has high theoretical specific capacity. For this respect, combining each advantage of BC and WO<sub>3</sub>·2H<sub>2</sub>O to improve the performance might bring novel and excellent properties. However, so far, to the best of our knowledge, nearly no works have been done in this aspect.

For decades, researchers have reported many ways to fabricate WO<sub>3</sub>/carbon materials, such as hydrothermal method, impregnation methods, and sol-gel method. Compared with these methods, as we previously reported, the radiation method can improve the contact between the doped materials and pristine carbon, and this method has been successfully applied in H<sub>2</sub> storage (Zhong et al., 2015, 2016). Obviously, good adhesion may improve the stability of hybrids and optimize the conduction of electrons, which will enhance the capacitive properties of the hybrids. But so far, no studies have been conducted on the preparation of metal oxides and carbon hybrid materials for supercapacitor applications by the irradiation method. To widen application of this method and further improve the capacitive performance, it is important to develop this method.

In this work, novel WO<sub>3</sub>·2H<sub>2</sub>O/BC hybrids were designed and fabricated by a facile  $\gamma$ -irradiation strategy. Morphologies and microstructures of the samples were investigated by XRD, SEM, TEM, and XPS, whereas CV, GCD, and EIS were carried out to study capacitive properties. The electrochemical results demonstrated that WO<sub>3</sub>·2H<sub>2</sub>O/BC hybrids delivered a high specific capacity (391 F g<sup>-1</sup> at 0.5 A g<sup>-1</sup>) and superior long-term stability (82% retention even after 10,000 cycles). The combination of bamboo (EDLC) and WO<sub>3</sub>·2H<sub>2</sub>O (pseudocapacitance) provided short ion diffusion path and fast electron transport, leading to a great supercapacitor.

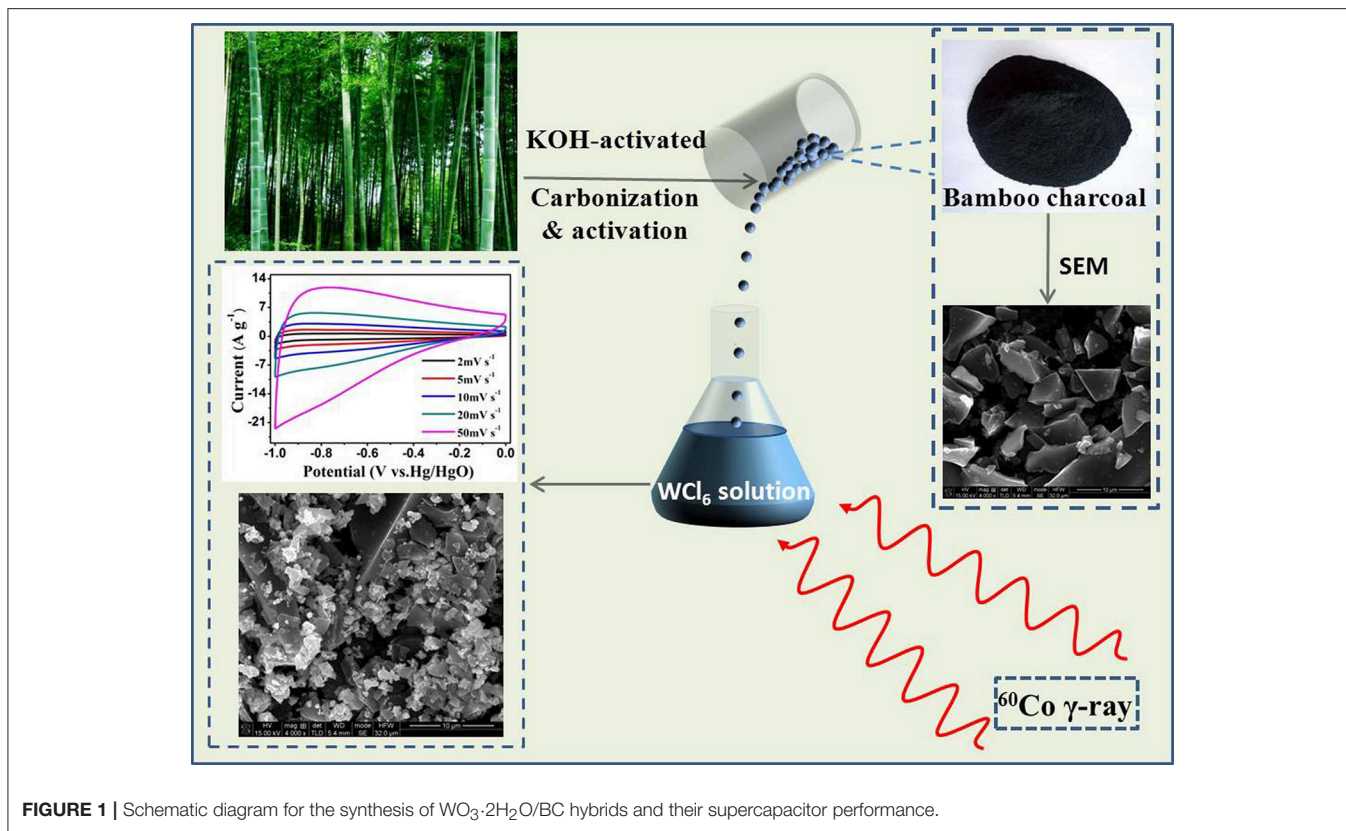
## EXPERIMENTAL DETAILS

### Synthesis of WO<sub>3</sub>·2H<sub>2</sub>O/BC Hybrids

All the reagents and solvents were analytical grade and used without further purification. In a typical process, WO<sub>3</sub>·2H<sub>2</sub>O/BC hybrids were prepared as follows. WCl<sub>6</sub> (3 mg) was added into isopropyl alcohol (20 mL) under stirring for 20 min in a glass vial at room temperature. Then, the BC monoliths (0.2 g) were slowly impregnated with 10 ml of WCl<sub>6</sub> solution. After 30 min of continuous stirring, 2-propanol was added with proper amount to scavenge H<sup>\*</sup> and OH<sup>\*</sup> radicals, which were generated during irradiation. The mixture was irradiated at room temperature with a <sup>60</sup>Co  $\gamma$ -ray source at a dose rate of 200 Gy min<sup>-1</sup>, and the total dose was 500 kGy. The product was collected by centrifugation and rinsed several times with DI water and ethanol, and then dried at 60°C for 12 h. **Figure 1** shows the schematic diagram for the synthesis of WO<sub>3</sub>·2H<sub>2</sub>O/BC hybrids and their supercapacitor performance. For comparison, bamboo charcoal was prepared by carbonization of natural bamboo with the KOH-modified method, as described elsewhere (Yang et al., 2014; Li and Wu, 2015).

### Material Characterization

The crystalline phase of WO<sub>3</sub>·2H<sub>2</sub>O/BC hybrids was examined by X-ray powder diffraction (XRD) employing monochromatized CuK $\alpha$  incident radiation. The morphology and microstructure were analyzed by using a field emission scanning electron microscope (FESEM, Nova 600i) with an attached energy dispersive X-ray spectroscopy (EDS)



analysis and transmission electron microscopy (TEM). X-ray photoelectron spectroscopy (XPS) was studied for detecting chemical composition and oxidation states of WO<sub>3</sub>·2H<sub>2</sub>O/BC hybrids.

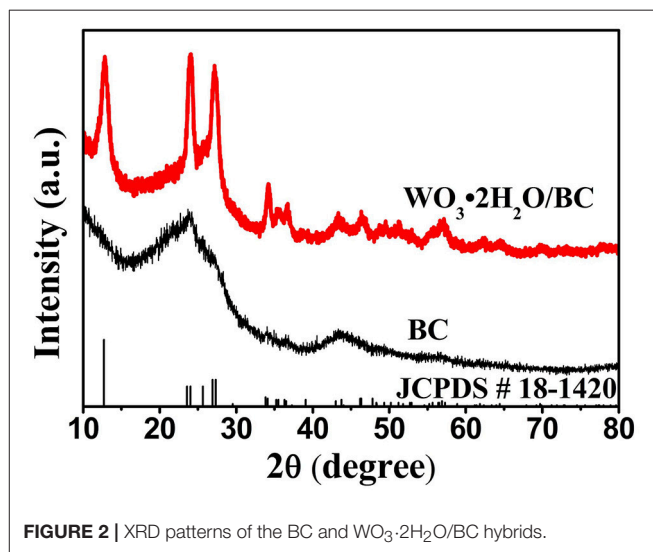
### Electrochemical Measurements

Electrochemical tests were carried out at room temperature in a conventional three-electrode configuration with 6 M KOH as an electrolyte using an electrochemical workstation (CHI 660E), WO<sub>3</sub>·2H<sub>2</sub>O/BC as a working electrode, platinum foil as a counter electrode, and Hg/HgO as a reference electrode. In electrochemical tests, WO<sub>3</sub>·2H<sub>2</sub>O/BC (80%) was mixed with acetylene black (10%) and polyvinylidene fluoride (PVDF, 10%) in N-methyl-2-pyrrolidone (NMP) to form slurry. Then the slurry was coated on glassy carbon to fabricate the working electrode. The potential range for CV tests is from -1 to 0 V, and the measurement range for EIS tests is between 0.1 Hz and 100 kHz with an AC amplitude of 5 mV.

## RESULTS AND DISCUSSION

### Characterization of WO<sub>3</sub>·2H<sub>2</sub>O/BC Hybrids

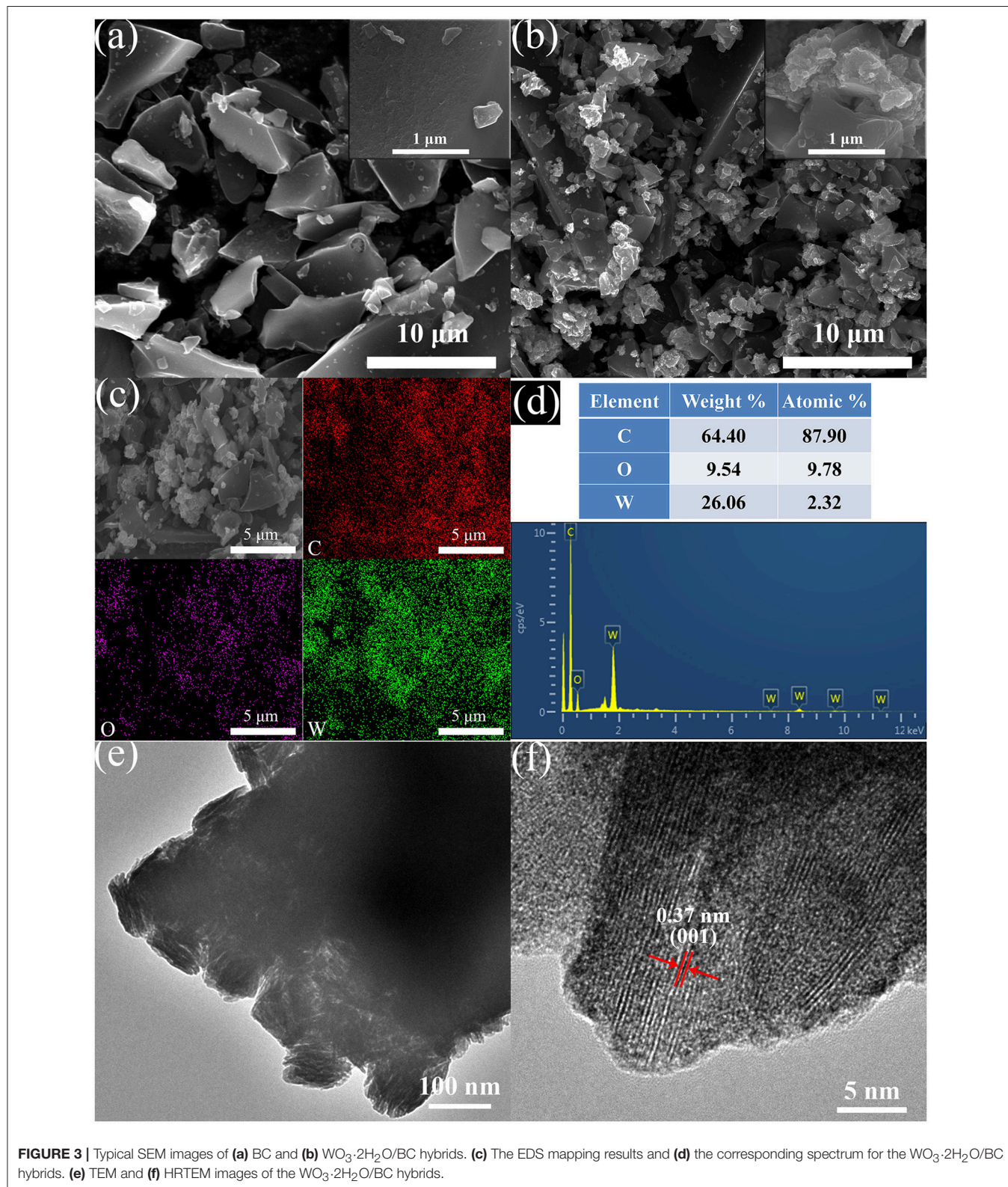
Crystal structures of the as-prepared BC and WO<sub>3</sub>·2H<sub>2</sub>O/BC hybrids were first studied by XRD. As shown in **Figure 2**, two broad peaks near 23 and 43° correspond to (002) and (100), respectively, which can be identified for the amorphous



forms of BC. For WO<sub>3</sub>·2H<sub>2</sub>O/BC hybrids, two broad peaks of BC also appeared, and all the peaks exclusively assigned to the characteristic structure of WO<sub>3</sub>·2H<sub>2</sub>O (JCPDS-00-18-1420). Furthermore, no other impurity phase peak can be detected, and the existence of strong and sharp peaks also indicates that WO<sub>3</sub>·2H<sub>2</sub>O/BC hybrids have high crystallinity. The structure of WO<sub>3</sub>·2H<sub>2</sub>O has been reported to be attractive as electrode

materials (Ma et al., 2015; Li et al., 2016; Mitchell et al., 2017). Crystalline WO<sub>3</sub> is much more stable than amorphous WO<sub>3</sub> due to the denser structure and lower dissolution rate

in electrolytes, which is a very important point in terms of practical applications (Liu et al., 2017). The diffraction pattern of WO<sub>3</sub>·2H<sub>2</sub>O/BC hybrids is the combination of the peaks from



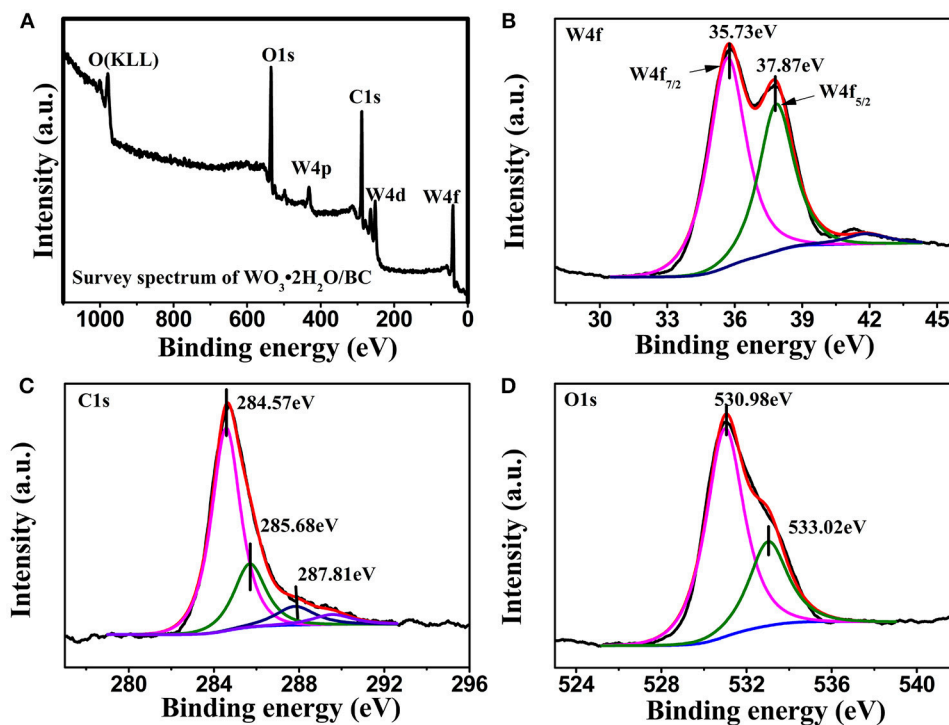


**FIGURE 4** | The XPS spectra of WO<sub>3</sub>·2H<sub>2</sub>O/BC (A) survey scan spectrum, (B) W 4f core level spectrum, (C) C 1s core level spectrum, and (D) O 1s core level spectrum.

BC and WO<sub>3</sub>·2H<sub>2</sub>O, demonstrating the successful composite. However, for the amorphous forms of BC, no distinct peaks of BC can be observed in WO<sub>3</sub>·2H<sub>2</sub>O/BC hybrids. Nevertheless, the presence of BC in the WO<sub>3</sub>·2H<sub>2</sub>O/BC hybrids can be confirmed by the results of SEM, TEM, and XPS.

The surface morphologies of BC and WO<sub>3</sub>·2H<sub>2</sub>O/BC hybrids were characterized by SEM and TEM. As shown in **Figure 3a**, we can clearly see that the BC has smooth surface and irregular forms. **Figure 3b** shows the morphology of WO<sub>3</sub>·2H<sub>2</sub>O/BC hybrids, and the skeleton of BC can be clearly seen with a random distribution of WO<sub>3</sub>·2H<sub>2</sub>O. EDS mapping was further used to demonstrate the formation of WO<sub>3</sub>·2H<sub>2</sub>O/BC hybrids, and is shown in **Figure 3c**. Obviously, the C, W, and O elements exist in WO<sub>3</sub>·2H<sub>2</sub>O/BC hybrids, and this result is in accord with the EDS spectrum shown in **Figure 3d**. As shown in **Figures 3e,f**, TEM and high-resolution TEM (HRTEM) micrographs further indicate microscopic structures of WO<sub>3</sub>·2H<sub>2</sub>O/BC hybrids. The TEM image of WO<sub>3</sub>·2H<sub>2</sub>O/BC hybrids clearly reveals that WO<sub>3</sub>·2H<sub>2</sub>O is successfully connected to BC. The HRTEM image of WO<sub>3</sub>·2H<sub>2</sub>O/BC (**Figure 3f**) shows that the spacing between adjacent lattice planes is 0.37 nm, corresponding to the (001) plane of WO<sub>3</sub>·2H<sub>2</sub>O, indicating that WO<sub>3</sub>·2H<sub>2</sub>O grows preferentially along (001) (Mitchell et al., 2017). Therefore, WO<sub>3</sub>·2H<sub>2</sub>O/BC hybrids can be successfully synthesized via a simple  $\gamma$ -irradiation method, in which WO<sub>3</sub>·2H<sub>2</sub>O is sufficiently connected to BC. And the robust contact between WO<sub>3</sub> and BC can be maintained by ultrasound for 30 min without WO<sub>3</sub>

shed (see **Figure 3e**). This great interfacial contact between WO<sub>3</sub>·2H<sub>2</sub>O and BC may be possibly favorable for the electronic transport process, thus resulting in the enhanced supercapacitor performance (Cai et al., 2014; Chu et al., 2017; Liu et al., 2018a,b). To further check the surface chemical composition of WO<sub>3</sub>·2H<sub>2</sub>O/BC hybrids, XPS measurements were carried out.

The detailed composition and surface valence state of WO<sub>3</sub>·2H<sub>2</sub>O/BC hybrids was probed by XPS measurements. **Figure 4A** shows the survey scan spectrum of the WO<sub>3</sub>·2H<sub>2</sub>O/BC hybrids, and only W, O, and C elements exist in the hybrids without evidence of any other impurity atoms. **Figure 4B** shows the XPS spectrum of the W 4f doublet peak in the high-resolution scan. The peaks located at 37.87 and 35.73 eV are attributable to the W 4f<sub>5/2</sub> and W 4f<sub>7/2</sub>, respectively. The observed energy position of the doublet is in accord with the previous report for the W<sup>6+</sup> oxidation state (Shinde et al., 2016; Xu et al., 2016; Liu et al., 2017; Wu and Yao, 2017). The splitting between W 4f<sub>7/2</sub> and W 4f<sub>5/2</sub> is 2.14 eV, demonstrating a typical state of W<sup>6+</sup> in WO<sub>3</sub>·2H<sub>2</sub>O/BC hybrids, which is well analogous to the XRD study. The XPS spectrum of C 1s from the WO<sub>3</sub>·2H<sub>2</sub>O/BC hybrids (see **Figure 4C**) is also decomposed into three peaks at 284.57 eV (C–C), 285.68 eV (C–O), and 287.81 eV (C = O), suggesting that the bonding between carbon atoms of BC and oxygen atoms of WO<sub>3</sub>·2H<sub>2</sub>O improves the conductivity and accelerates charge transport for the hybrids (Cai et al., 2014;

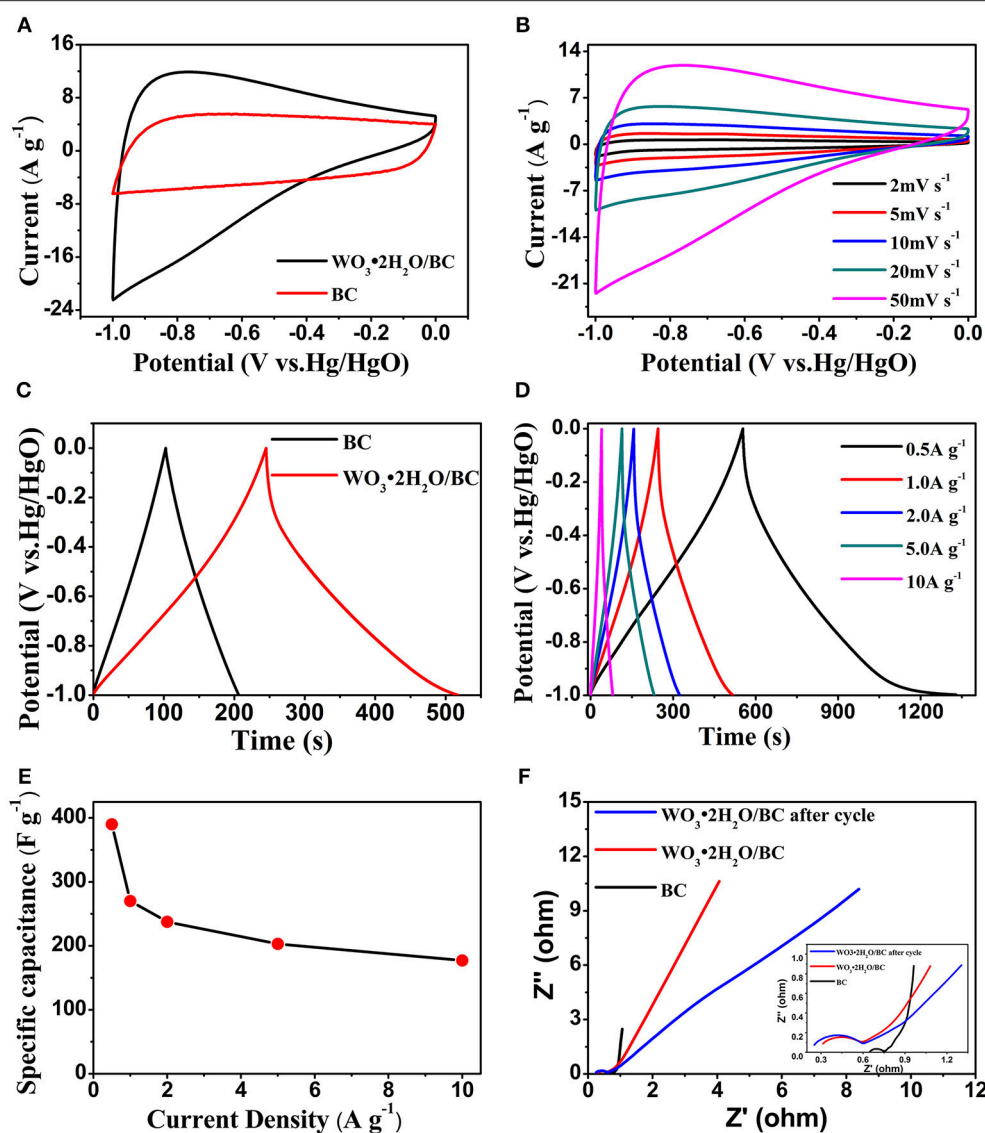


**FIGURE 5 |** (A) The CV curves of BC and WO<sub>3</sub>·2H<sub>2</sub>O/BC electrodes at a scan rate of 50 mV s<sup>-1</sup>. (B) The CV curves of the WO<sub>3</sub>·2H<sub>2</sub>O/BC electrode at different scan rates. (C) GCD curves of BC and WO<sub>3</sub>·2H<sub>2</sub>O/BC electrodes at a current density of 1 A g<sup>-1</sup>. (D) GCD curves of the WO<sub>3</sub>·2H<sub>2</sub>O/BC electrode at different current densities. (E) Specific capacitance of the WO<sub>3</sub>·2H<sub>2</sub>O/BC electrode at different current densities. (F) EIS of the BC and WO<sub>3</sub>·2H<sub>2</sub>O/BC electrodes.

Nayak et al., 2017). And the deconvolution peak of the O 1s spectrum can be resolved into two components of 530.98 and 533.02 eV (see **Figure 4D**). The low binding energy component at 530.98 eV is attributed to the O<sup>2-</sup> bond with wolfram, and the latter peak is assigned to OH<sup>-</sup> (Xing et al., 2016; Nayak et al., 2017).

## Electrochemical Performance of WO<sub>3</sub>·2H<sub>2</sub>O/BC Hybrids

The electrochemical performance of WO<sub>3</sub>·2H<sub>2</sub>O/BC hybrids was first investigated by the CV test. The CV curves of the BC and WO<sub>3</sub>·2H<sub>2</sub>O/BC electrodes are shown in **Figure 5A**. Compared with those of BC, the CV curves of WO<sub>3</sub>·2H<sub>2</sub>O/BC

changed from the rectangular shape to the “dolphin-like” shape, and nearly no obvious redox peaks detected are characteristic among various WO<sub>3</sub> (Reddy et al., 2015; Thind et al., 2016; He et al., 2017; Nayak et al., 2017). Moreover, the stored charge of the hybrids can be calculated by the enclosed area of the CV curve. The observed integrated area of the WO<sub>3</sub>·2H<sub>2</sub>O/BC electrode at the same current density is much larger than that of the BC electrode, suggesting the contribution of WO<sub>3</sub>·2H<sub>2</sub>O incorporation to the enhanced specific capacitance of WO<sub>3</sub>·2H<sub>2</sub>O/BC, and the combined effect of WO<sub>3</sub>·2H<sub>2</sub>O and BC is significant (Cai et al., 2014; Liu et al., 2018a). The results obtained here are also consistent with the SEM and TEM morphologies, suggesting that the WO<sub>3</sub>·2H<sub>2</sub>O/BC

hybrid morphology provides good contact facilitating the fast charge intercalation/deintercalation process, and the enhanced electronic conductivity after carbon incorporation contributes to the superior electrochemical performance. **Figure 5B** shows the CV curves of WO<sub>3</sub>·2H<sub>2</sub>O/BC in 6 M KOH at different scan rates (2, 5, 10, 20, and 50 mV s<sup>-1</sup>) over a potential window of -1 to 0 V. The corresponding CV curves of BC are provided in **Figure S1a**. The increased area under the curve with scan rate is clearly observed, indicating an

excellent capacitance behavior and high-rate capability of the electrode.

Charge-discharge measurements were conducted under galvanostatic conditions at different applied current densities. The GCD plots of the BC and WO<sub>3</sub>·2H<sub>2</sub>O/BC electrodes at a current density of 1 A g<sup>-1</sup> are presented in **Figure 5C**. According to the galvanostatic discharge curves, the specific capacitance ( $C_s$ , F g<sup>-1</sup>) of the electrode is calculated according to the following equation:

$$C_s(\text{F g}^{-1}) = \frac{I\Delta t}{m\Delta V}$$

where  $I$  (mA) represents the applied current,  $\Delta t$  (s) the discharge time,  $\Delta V$  (V) the potential window, and  $m$  (mg) the weight of the active material. In addition, the discharge time of WO<sub>3</sub>·2H<sub>2</sub>O/BC is much larger than that of BC, showing higher capacitance. And this result is also consistent with the CV tests. GCD curves of WO<sub>3</sub>·2H<sub>2</sub>O/BC and BC (**Figure S1b**) electrodes recorded at 0.5, 1, 2, 5, and 10 A g<sup>-1</sup> are shown in **Figure 5D**. With the increasing charging and discharging currents, a highly linear and nearly symmetric relationship between the potential and time was also observed, suggesting the desired fast charging and discharging property of the materials. No obvious internal resistance (IR) drop of the BC (**Figure S1b**) and WO<sub>3</sub>·2H<sub>2</sub>O/BC electrodes was observed for any of the curves, which indicates high conductivity of the materials. The higher  $C_s$  of WO<sub>3</sub>·2H<sub>2</sub>O/BC is due to the combined effects between WO<sub>3</sub>·2H<sub>2</sub>O and BC (Chu et al., 2017), and the superior electrochemical performance may be mainly attributed to the enhanced electronic conductivity after carbon incorporation. As shown in **Figure 5E**, the calculated  $C_s$  of

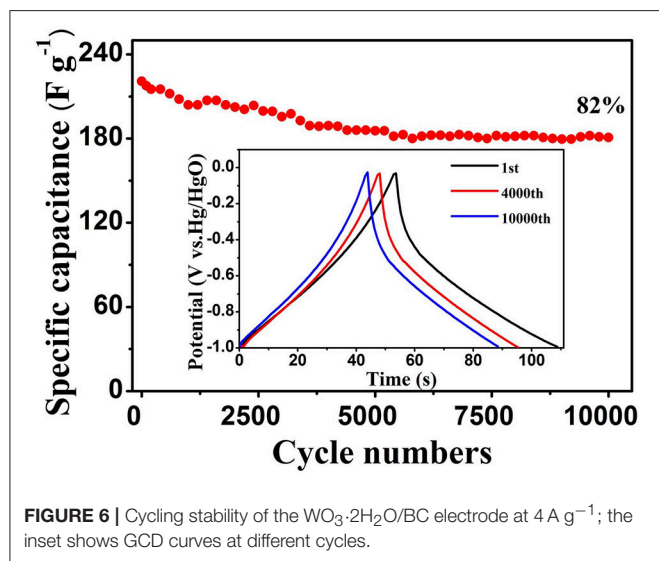


**FIGURE 6** | Cycling stability of the WO<sub>3</sub>·2H<sub>2</sub>O/BC electrode at 4 A g<sup>-1</sup>; the inset shows GCD curves at different cycles.

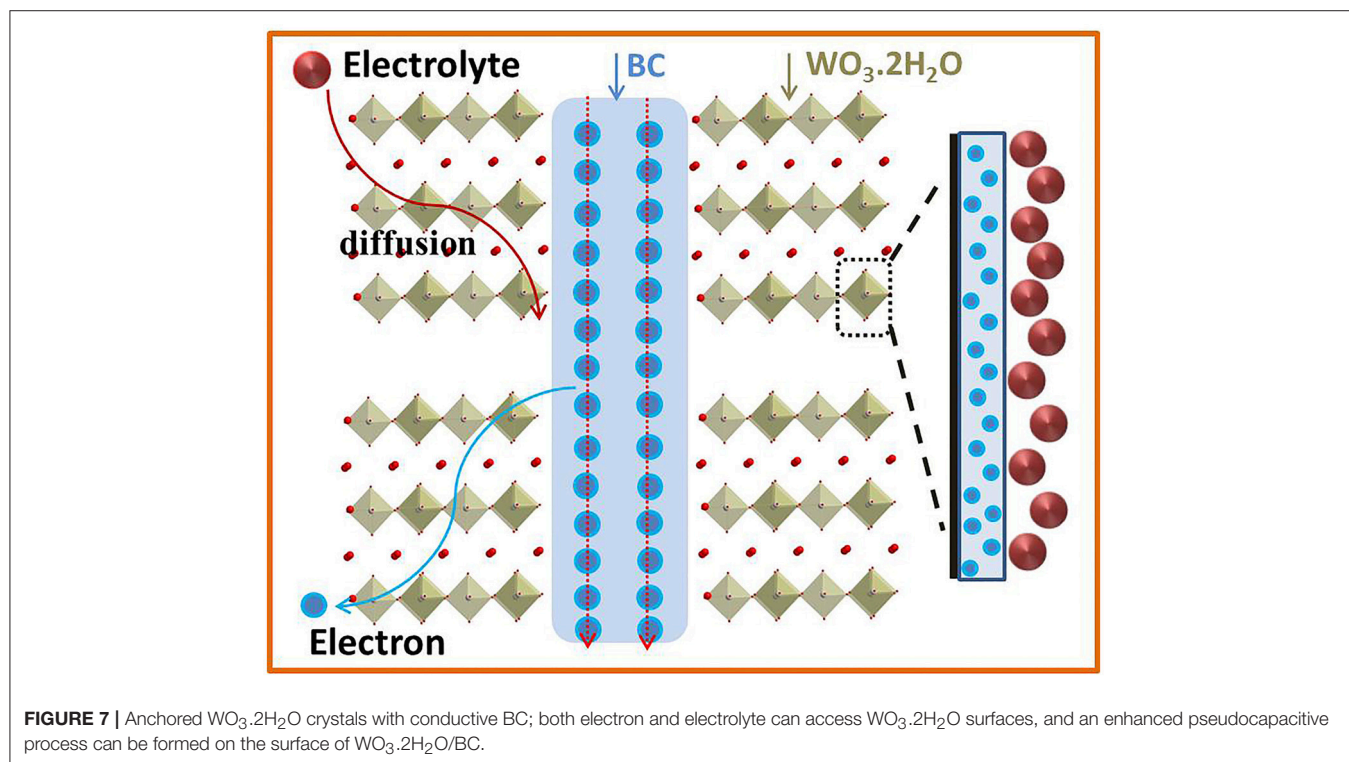


**FIGURE 7** | Anchored WO<sub>3</sub>·2H<sub>2</sub>O crystals with conductive BC; both electron and electrolyte can access WO<sub>3</sub>·2H<sub>2</sub>O surfaces, and an enhanced pseudocapacitive process can be formed on the surface of WO<sub>3</sub>·2H<sub>2</sub>O/BC.

WO<sub>3</sub>·2H<sub>2</sub>O/BC are 391, 270, 227.5, 203, and 177 F g<sup>-1</sup> at current densities of 0.5, 1, 2, 5, and 10 A g<sup>-1</sup>, respectively, demonstrating that the C<sub>s</sub> decreases with increasing current density (Shinde et al., 2017). The coulombic efficiency of WO<sub>3</sub>·2H<sub>2</sub>O/BC hybrids is ~100%, exhibiting a good reversibility during the charge/discharge process. Furthermore, ~45% of the capacitance was retained when the current density increased from 0.5 to 10 A g<sup>-1</sup>, higher than the reported graphene nanosheets-tungsten oxides composites (34% capacitance retention from 0.1 to 5 A g<sup>-1</sup>), owing to the sluggish intercalation/deintercalation process of WO<sub>3</sub>·2H<sub>2</sub>O/BC at a high scan rate (Cai et al., 2014). These results are comparable to those of WO<sub>3</sub>-carbon-based electrodes in earlier reports (Table S1). To sum up, the enhancement in the electrochemical performance for WO<sub>3</sub>·2H<sub>2</sub>O/BC hybrids is mainly explained as follows: (i) the great interfacial contact between WO<sub>3</sub>·2H<sub>2</sub>O and BC provides short ion diffusion paths and the rapid electronic transports; (ii) the superior electrochemical performance may be mainly attributed to the enhanced electronic conductivity after carbon incorporation.

The EIS study was conducted to elucidate electrical conductivity and ion transfer features of BC and WO<sub>3</sub>·2H<sub>2</sub>O/BC electrodes. Electrochemical impedance characteristics of the electrode were investigated in a frequency range from 100 kHz to 0.1 Hz with an AC amplitude of 5 mV in 6 M KOH electrolyte. Figure 5F displays the typical Nyquist plots of these BC and WO<sub>3</sub>·2H<sub>2</sub>O/BC samples and the inset figure shows the magnified plots. For all the Nyquist plots, a semicircle can be seen in the high-frequency region, whereas in the low-frequency region, a straight line can be found. According to the previous reports (Sun et al., 2015; Chu et al., 2017; Yao C. et al., 2017), a straight line should relate to the ion diffusion into the active electrode (Z<sub>w</sub>), whereas the semicircle can be assigned to the charge transfer resistance (R<sub>ct</sub>) owing to the faradic and non-faradic reactions at the electrode/electrolyte interface. After doped with WO<sub>3</sub>·2H<sub>2</sub>O, the WO<sub>3</sub>·2H<sub>2</sub>O/BC electrode exhibits larger R<sub>ct</sub> and Z<sub>w</sub> than BC, mainly due to the poor electric conductivity of WO<sub>3</sub>·2H<sub>2</sub>O (Shinde et al., 2017). For comparison of first cycle and after 10,000 cycles, the R<sub>ct</sub> of WO<sub>3</sub>·2H<sub>2</sub>O/BC hybrids after the cycle is slightly larger than the value before the cycle, suggesting that WO<sub>3</sub>·2H<sub>2</sub>O/BC hybrids have good stability (Cai et al., 2014).

The cycling stability is the key factor to evaluate the practical applications of electrodes. To explore this, the cycle stability of WO<sub>3</sub>·2H<sub>2</sub>O/BC hybrids was further investigated by repeating the GCD test between -1 and 0 V at 4 A g<sup>-1</sup> for 10,000 cycles (Figure 6). Impressively, after 10,000 cycles, the initial C<sub>s</sub> (220.8 F g<sup>-1</sup>) of the WO<sub>3</sub>·2H<sub>2</sub>O/BC electrode slightly declined to 180.8 F g<sup>-1</sup>, and approximately 82% of the initial capacitance was retained. The inset shows the 1st, 4,000th and 10,000th GCD curves, respectively, indicating that the GCD profiles retain superior linearity and symmetry even after 10,000 cycles. Compared with other studies, to the best of our knowledge, in our work, the WO<sub>3</sub>·2H<sub>2</sub>O/BC hybrid electrode shows comparable cycling stability (Table S1); moreover the BC used in our work is much cheaper. Therefore, the combined effect of WO<sub>3</sub>·2H<sub>2</sub>O and BC accelerates the sufficient ion diffusion. This result confirms that the prepared WO<sub>3</sub>·2H<sub>2</sub>O/BC hybrids were highly stable as a novel supercapacitor electrode.

Figure 7 shows the storage mechanism of WO<sub>3</sub>·2H<sub>2</sub>O/BC hybrids. Briefly, the mechanism of WO<sub>3</sub>·2H<sub>2</sub>O/BC hybrids can be described as follows. First, the high conductivity of BC facilitates the rapid transfer of electrons. Secondly, after the  $\gamma$ -irradiation process, the good contact of BC and WO<sub>3</sub>·2H<sub>2</sub>O guarantees a low internal resistance between BC and WO<sub>3</sub>·2H<sub>2</sub>O, and also facilitates the transmission of low-loss electrons to the anchored WO<sub>3</sub>·2H<sub>2</sub>O. Thirdly, the structure of WO<sub>3</sub>·2H<sub>2</sub>O facilitates ion adsorption and insertion in the electrolyte, so an enhanced pseudocapacitor process can be formed on the surface of WO<sub>3</sub>·2H<sub>2</sub>O. In addition, the good contact of BC and WO<sub>3</sub> also makes it difficult for WO<sub>3</sub>·2H<sub>2</sub>O to agglomerate during the charge/discharge process, and also ensures the long-term stability of WO<sub>3</sub>·2H<sub>2</sub>O/BC hybrids. All of these characteristics of WO<sub>3</sub>·2H<sub>2</sub>O/BC hybrids contribute to the high specific capacitance and good cycling stability.

## CONCLUSIONS

In summary, we successfully synthesized WO<sub>3</sub>·2H<sub>2</sub>O/BC hybrids via a facile  $\gamma$ -irradiation method. The electrochemical capacitive behaviors of the WO<sub>3</sub>·2H<sub>2</sub>O/BC hybrids and BC have been demonstrated in 6 M KOH electrolyte between -1 and 0 V. In comparison with the BC electrode, the WO<sub>3</sub>·2H<sub>2</sub>O/BC hybrid electrode showed a higher C<sub>s</sub> (391 F g<sup>-1</sup> at 0.5 A g<sup>-1</sup>) and superior cycling performance (approximately 82% retention even after 10,000 cycles). The excellent performance achieved by the WO<sub>3</sub>·2H<sub>2</sub>O/BC hybrid electrode is owing to the combined effect of BC with good conductivity and WO<sub>3</sub>·2H<sub>2</sub>O with superior pseudocapacitive behavior. This  $\gamma$ -irradiation method would also pave a new way of designing other conducting semiconductors as promising electrode materials with enhanced performance for energy storage device applications.

## ETHICS STATEMENT

On behalf of, and having obtained permission from all the authors, I declare that: (a) the material has not been published in whole or in part elsewhere; (b) the paper is not currently being considered for publication elsewhere; (c) all authors have been personally and actively involved in substantive work leading to the report, and will hold themselves jointly and individually responsible for its content; I testify to the accuracy of the above on behalf of all the authors.

## AUTHOR CONTRIBUTIONS

YT developed the concept. XDL designed the experiments. FY and JJ conducted the experiments. RM and XCL built the cells and carried out the performance characterizations. ZF and CW supervised the research. FY and JJ co-wrote the manuscript. All authors discussed the results and commented on the manuscript.

## FUNDING

This study was financially supported by the Research Program of Sichuan province (grant no. 2016GZ0235) and the Development

Foundation of China Academy of Engineering Physics (grant no. 2015B0302003) and the national key scientific instrument and equipment development project of China (grant no. 2014YQ090709).

## ACKNOWLEDGMENTS

We acknowledge Q. Yang, Y. Zeng, and J. Li (Science and Technology on plasma physics Laboratory, Research Centre

of Laser Fusion, China Academy of Engineering physics, Mianyang, China) for the TEM, SEM, and XRD measurements, respectively.

## SUPPLEMENTARY MATERIAL

The Supplementary Material for this article can be found online at: <https://www.frontiersin.org/articles/10.3389/fchem.2018.00290/full#supplementary-material>

## REFERENCES

- Boyjoo, Y., Cheng, Y., Zhong, H., Tian, H., Pan, J., Pareek, V. K., et al. (2017). From waste Coca Cola® to activated carbons with impressive capabilities for CO<sub>2</sub> adsorption and supercapacitors. *Carbon* 116, 490–499. doi: 10.1016/j.carbon.2017.02.030
- Cai, Y., Wang, Y., Deng, S., Chen, G., Li, Q., Han, B., Han, R., Wang, Y., et al. (2014). Graphene nanosheets-tungsten oxides composite for supercapacitor electrode. *Ceram. Int.* 40, 4109–4116. doi: 10.1016/j.ceramint.2013.08.065
- Chu, J., Lu, D., Wang, X., Wang, X., and Xiong, S. (2017). WO<sub>3</sub> nanoflower coated with graphene nanosheet: synergetic energy storage composite electrode for supercapacitor application. *J. Alloys Compd.* 702, 568–572. doi: 10.1016/j.jallcom.2017.01.226
- Dai, S., Liu, Z., Zhao, B., Zeng, J., Hu, H., Zhang, Q., et al. (2018). A high-performance supercapacitor electrode based on N-doped porous grapheme. *J. Power Sources* 387, 43–48. doi: 10.1016/j.jpowsour.2018.03.055
- Dai, S., Zhao, B., Qu, C., Chen, D., Dang, D., Song, B., et al. (2017). Controlled synthesis of three-phase Ni<sub>3</sub>S<sub>2</sub>/rGO nanoflake electrodes for hybrid supercapacitors with high energy and power density. *Nano Energy* 33, 522–531. doi: 10.1016/j.nanoen.2017.01.056
- He, G., Ling, M., Han, X., Abou El Amaiem, D. I., Shao, Y., Li, Y., et al. (2017). Self-standing electrodes with core-shell structures for high-performance supercapacitors. *Energy Storage Mater.* 9, 119–125. doi: 10.1016/j.ensm.2017.07.005
- Li, H., Wang, J., Shi, Q., Zhang, M., Hou, C., Shi, G., et al. (2016). Constructing three-dimensional quasi-vertical nanosheet architectures from self-assemble two-dimensional WO<sub>3</sub>-2H<sub>2</sub>O for efficient electrochromic devices. *Appl. Surf. Sci.* 380, 281–287. doi: 10.1016/j.apsusc.2016.01.009
- Li, J., and Wu, Q. (2015). Water bamboo-derived porous carbons as electrode materials for supercapacitors. *New J. Chem.* 39, 3859–3864. doi: 10.1039/c4nj01853b
- Liu, B., Wang, Y., Jiang, H., and Zou, B. X. (2017). WO<sub>3</sub> nanowires on graphene sheets as negative electrode for supercapacitors. *J. Nanomater.* 24, 109–117. doi: 10.1155/2017/2494109
- Liu, X., Sheng, G., Zhong, M., and Zhou, X. (2018a). Hybrid nanowires and nanoparticles of WO<sub>3</sub> in a carbon aerogel for supercapacitor applications. *Nanoscale* 10, 4209–4217. doi: 10.1039/c7nr07191d
- Liu, X., Sheng, G., Zhong, M., and Zhou, X. (2018b). Dispersed and size-selected WO<sub>3</sub> nanoparticles in carbon aerogel for supercapacitor applications. *Mater. Design* 141, 220–229. doi: 10.1016/j.matdes.2017.12.038
- Lu, X., Zhai, T., Zhang, X., Shen, Y., Yuan, L., Hu, B., et al. (2012). WO<sub>3-x</sub>/Au/MnO<sub>2</sub> core-shell nanowires on carbon fabric for high-performance flexible supercapacitors. *Adv. Mater.* 24, 938–944. doi: 10.1002/adma.201104113
- Ma, L., Zhou, X., Xu, L., Xu, X., Zhang, L., Ye, C., et al. (2015). Hydrothermal preparation and supercapacitive performance of flower-like WO<sub>3</sub>-H<sub>2</sub>O/reduced graphene oxide composite. *Colloids Surf. A* 481, 609–615. doi: 10.1016/j.colsurfa.2015.06.040
- Mitchell, J. B., Lo, W. C., Genc, A., LeBeau, J., and Augustyn, V. (2017). Transition from battery to pseudocapacitor behavior via structural water in tungsten oxide. *Chem. Mater.* 29, 3928–3937. doi: 10.1021/acs.chemmater.6b05485
- Nayak, A. K., Das, A. K., and Pradhan, D. (2017). High performance solid-State asymmetric supercapacitor using green synthesized graphene-WO<sub>3</sub> nanowires nanocomposite. *ACS Sustainable Chem. Eng.* 5, 10128–10138. doi: 10.1021/acsschemeng.7b02135
- Pang, L., Zou, B., Zou, Y., Han, X., Cao, L., Wang, W., et al. (2016). A new route for the fabrication of corn starch-based porous carbon as electrochemical supercapacitor electrode material. *Colloids Surf. A* 504, 26–33. doi: 10.1016/j.colsurfa.2016.05.049
- Qiu, M., Sun, P., Shen, L., Wang, K., Song, S., Yu, X., et al. (2016). WO<sub>3</sub> nanoflowers with excellent pseudo-capacitive performance and the capacitance contribution analysis. *J. Mater. Chem.* 4, 7266–7273. doi: 10.1039/c6ta00237d
- Reddy, B. N., Kumar, P. N., and Deepa, M. (2015). A Poly (3,4-ethylenedioxyppyrrrole)-Au@WO<sub>3</sub>-based electrochromic pseudocapacitor. *ChemPhysChem* 16, 377–389. doi: 10.1002/cphc.201402625
- Shinde, P. A., Lokhande, A. C., Chodankar, N. R., Patil, A. M., Jin, H. K., and Lokhande, C. D. (2017). Temperature dependent surface morphological modifications of hexagonal WO<sub>3</sub> thin films for high performance supercapacitor application. *Electrochim. Acta* 224, 397–404. doi: 10.1016/j.electacta.2016.12.066
- Shinde, P. A., Lokhande, V. C., Chodankar, N. R., Ji, T., and Kim, J. H., Lokhande, C. D. (2016). Enhanced electrochemical performance of monoclinic WO<sub>3</sub> thin film with redox additive aqueous electrolyte. *J. Colloid Interface Sci.* 483, 261–267. doi: 10.1016/j.jcis.2016.08.011
- Sun, P., Deng, Z., Yang, P., Yu, X., Chen, Y., Liang, Z., et al. (2015). Freestanding CNT-WO<sub>3</sub> hybrid electrodes for flexible asymmetric supercapacitors. *J. Mater. Chem.* 3, 12076–12080. doi: 10.1039/c5ta02316e
- Thind, S. S., Chang, X., Wentzell, J. S., and Chen, A. (2016). High-performance supercapacitor based on tantalum iridium oxides supported on tungsten oxide nanoplatelets. *Electrochem. Commun.* 67, 1–5. doi: 10.1016/j.elecom.2016.03.002
- Wang, C.-H., Wen, W.-C., Hsu, H.-C., and Yao, B.-Y., et al. (2016). High-capacitance KOH-activated nitrogen-containing porous carbon material from waste coffee grounds in supercapacitor. *Adv. Polym. Technol.* 27, 1387–1395. doi: 10.1016/j.apt.2016.04.033
- Wang, F., Zhan, X., Cheng, Z., Wang, Z., Wang, Q., Xu, K., et al. (2015). Tungsten oxide@polypyrrole core-shell nanowire arrays as novel negative electrodes for asymmetric supercapacitors. *Small* 11, 749–755. doi: 10.1002/sml.201402340
- Wang, J. G., Liu, H., Zhang, X., Li, X., Liu, X., Kang, F., et al. (2018). Green synthesis of hierarchically porous carbon nanotubes as advanced materials for high-efficient energy storage. *Small* 14:e1703950. doi: 10.1002/sml.201703950
- Wang, K., Wu, H., Meng, Y., and Wei, Z. (2014). Conducting polymer nanowire arrays for high performance supercapacitors. *Small* 10, 14–31. doi: 10.1002/sml.201301991
- Wang, R., Wang, P., Yan, X., Lang, J., Chao, P., and Xue, Q. (2012). Promising porous carbon derived from celctue leaves with outstanding supercapacitance and CO<sub>2</sub> capture performance. *ACS Appl. Mater. Interfaces* 4, 5800–5806. doi: 10.1021/am302077c
- Wang, W., Wang, X., Wang, X., Yang, L., Wu, Z., Xia, S., et al. (2013). Cr (VI) removal from aqueous solution with bamboo charcoal chemically modified by iron and cobalt with the assistance of microwave. *J. Environ. Sci.* 25, 1726–1735. doi: 10.1016/s1001-0742(12)60247-2
- Wang, Y. H., Wang, C. C., Cheng, W. Y., and Lu, S. Y. (2014). Dispersing WO<sub>3</sub> in carbon aerogel makes an outstanding supercapacitor electrode material. *Carbon* 69, 287–293. doi: 10.1016/j.carbon.2013.12.027

- Wu, X., and Yao, S. (2017). Flexible electrode materials based on WO<sub>3</sub> nanotube bundles for high performance energy storage devices. *Nano Energy* 42, 143–150. doi: 10.1016/j.nanoen.2017.10.058
- Xiao, X., Ding, T., Yuan, L., Shen, Y., Zhong, Q., Zhang, X., et al. (2012). WO<sub>3-x</sub>/MoO<sub>3-x</sub> core/shell nanowires on carbon fabric as an anode for all-solid-state asymmetric supercapacitors. *Adv. Energy Mater.* 2, 1328–1332. doi: 10.1002/aenm.201200380
- Xing, L. L., Huang, K. J., and Fang, L. X. (2016). Preparation of layered graphene and tungsten oxide hybrids for enhanced performance supercapacitors. *Dalton Trans.* 45, 17439–17446. doi: 10.1039/c6dt03719d
- Xu, J., Li, Y., Wang, L., Cai, Q., Li, Q., Gao, B., et al. (2016). High-energy lithium-ion hybrid supercapacitors composed of hierarchical urchin-like WO<sub>3</sub>/C anodes and MOF-derived polyhedral hollow carbon cathodes. *Nanoscale* 8, 16761–16768. doi: 10.1039/c6nr05480c
- Xu, L., Zhao, Y., Lian, J., Xu, Y., Bao, J., Qiu, J., et al. (2017). Morphology controlled preparation of ZnCo<sub>2</sub>O<sub>4</sub> nanostructures for asymmetric supercapacitor with ultrahigh energy density. *Energy* 123, 296–304. doi: 10.1016/j.energy.2017.02.018
- Yang, C. S., Jang, Y. S., and Jeong, H. K. (2014). Bamboo-based activated carbon for supercapacitor applications. *Curr. Appl. Phys.* 14, 1616–1620. doi: 10.1016/j.cap.2014.09.021
- Yao, C., Wei, B. B., Li, H. H., Wang, G. F., Han, Q., Ma, H., et al. (2017). Carbon-encapsulated tungsten oxide nanowires as stable and high-rate anode for flexible asymmetric supercapacitors. *J. Mater. Chem.* 5, 51–56. doi: 10.1010.1039/C6TA08274B
- Yao, S., Zheng, X., Zhang, X., Xiao, H., Qu, F., Wu, X., et al. (2017). Facile synthesis of flexible WO<sub>3</sub> nanofibers as supercapacitor electrodes. *Mater. Lett.* 186, 94–97. doi: 10.1016/j.matlet.2016.09.085
- Yi, Z., Xu, X., Kang, X., Zhao, Y., Zhang, S., Yao, W., et al. (2017). Fabrication of well-aligned ZnO@Ag nanorod arrays with effective charge transfer for surface-enhanced Raman scattering. *Surf. Coat. Technol.* 324, 257–263. doi: 10.1016/j.surfcoat.2017.05.084
- Yu, S., Liu, D., Zhao, S., Bao, B., Jin, C., Huang, W., et al. (2015). Synthesis of wood derived nitrogen-doped porous carbon-polyaniline composites for supercapacitor electrode materials. *Rsc Adv.* 5, 30943–30949. doi: 10.1039/C5RA01949D
- Yuksel, R., Durucan, C., and Unalan, H. E. (2016). Ternary nanocomposite SWNT/WO<sub>3</sub>/PANI thin film electrodes for supercapacitors. *J. Alloys Compd.* 658, 183–189. doi: 10.1016/j.jallcom.2015.10.216
- Zeng, Z., Liu, Y., Zhang, W., Chevva, H., and Wei, J. (2017). Improved supercapacitor performance of MnO<sub>2</sub>-electrospun carbon nanofibers electrodes by mT magnetic field. *J. Power Sources* 358, 22–28. doi: 10.1016/j.jpowsour.2017.05.008
- Zhang, Q., Zhao, B., Wang, J., Qu, C., Sun, H., Zhang, K., et al. (2012). High-performance hybrid supercapacitors based on self-supported 3D ultrathin porous quaternary Zn-Ni-Al-Co oxide nanosheets. *Nano Energy* 28, 475–485. doi: 10.1016/j.nanoen.2016.08.049
- Zhang, Y., and Park, S. J. (2017). Incorporation of RuO<sub>2</sub> into charcoal-derived carbon with controllable microporosity by CO<sub>2</sub> activation for high-performance supercapacitor. *Carbon* 122, 287–297. doi: 10.1016/j.carbon.2017.06.085
- Zhang, Y., Yao, Q. Q., Gao, H. L., Zhang, L. S., Wang, L. Z., Zhang, A. Q., et al. (2015). Synthesis and electrochemical performance of MnO<sub>2</sub>/BC composite as active materials for supercapacitors. *J. Anal. Appl. Pyrolysis* 111, 233–237. doi: 10.1016/j.jaap.2014.11.002
- Zhang, Z., Wang, X., Wang, Y., Xia, S., Chen, L., Zhang, Y., et al. (2013). Pb (II) removal from water using Fe-coated bamboo charcoal with the assistance of microwaves. *J. Environ. Sci.* 25, 1044–1053. doi: 10.1016/S1001-0742(12)60144-2
- Zhao, B., Zhang, L., Zhang, Q., Chen, D., Chen, Y., Deng, X., et al. (2017). Rational design of nickel hydroxide-based nanocrystals on graphene for ultrafast energy storage. *Adv. Energy Mater.* 2017:1702247. doi: 10.1002/aenm.201702247
- Zhao, Y., Hu, L., Zhao, S., and Wu, L. (2016). Preparation of MnCo<sub>2</sub>O<sub>4</sub>@Ni(OH)<sub>2</sub> core-shell flowers for asymmetric supercapacitor materials with ultrahigh specific capacitance. *Adv. Funct. Mater.* 26, 4085–4093. doi: 10.1002/adfm.201600494
- Zhao, Y., Xu, L., Yan, J., Yan, W., Wu, C., Lian, J., et al. (2017). Facile preparation of NiFe<sub>2</sub>O<sub>4</sub>/MoS<sub>2</sub> composite material with synergistic effect for high performance supercapacitor. *J. Alloy. Compd.* 726, 608–617. doi: 10.1016/j.jallcom.2017.07.327
- Zhao, Y., Yuan, M., Chen, Y., Yan, J., Xu, L., Huang, Y., et al. (2018). Construction of molybdenum dioxide nanosheets coated on the surface of nickel ferrite nanocrystals with ultrahigh specific capacity for hybrid supercapacitor. *Electrochimica Acta* 260, 439–448. doi: 10.1016/j.electacta.2017.12.053
- Zhong, M., Fu, Z., Huang, W., Yang, X., and Liu, M. (2015). Fabrication of porous Pd/C microspheres in carbon aerogels by radiation method. *Mater. Lett.* 139, 314–317. doi: 10.1016/j.matlet.2014.10.098
- Zhong, M., Fu, Z., Huang, W., Yang, X., and Liu, M. (2016). A solution-phase synthesis method to prepare Pd doped carbon aerogels for hydrogen storage. *RSC Adv.* 5, 20966–20971. doi: 10.1039/c4ra16505e
- Zhu, J., and He, J. (2012). Facile synthesis of graphene-wrapped honeycomb MnO<sub>2</sub> nanospheres and their application in supercapacitors. *ACS Appl. Mater. Interfaces* 4, 1770–1776. doi: 10.1021/am3000165

**Conflict of Interest Statement:** The authors declare that the research was conducted in the absence of any commercial or financial relationships that could be construed as a potential conflict of interest.

Copyright © 2018 Yang, Jia, Mi, Liu, Fu, Wang, Liu and Tang. This is an open-access article distributed under the terms of the Creative Commons Attribution License (CC BY). The use, distribution or reproduction in other forums is permitted, provided the original author(s) and the copyright owner(s) are credited and that the original publication in this journal is cited, in accordance with accepted academic practice. No use, distribution or reproduction is permitted which does not comply with these terms.